

# Fast Surface Dynamics on a Metallic Glass Nanowire

*AUTHOR NAMES: Debaditya Chatterjee<sup>1</sup>, Ajay Annamareddy<sup>1</sup>, Jittisa Ketkaew<sup>2</sup>, Jan Schroers<sup>2</sup>, Dane Morgan<sup>1</sup>, Paul M. Voyles<sup>1\*</sup>*

## AUTHOR ADDRESSES:

<sup>1</sup>Department of Materials Science and Engineering, University of Wisconsin – Madison, Madison WI 53706, USA.

<sup>2</sup> Department of Mechanical Engineering and Materials Science, Yale University, New Haven, CT 06520, USA.

\*Corresponding author. Email: paul.voyles@wisc.edu

## ABSTRACT

The dynamics near the surface of glasses can be much faster than in the bulk. We have studied the surface dynamics of a Pt-based metallic glass using electron correlation microscopy with sub-nanometer resolution. Our studies show a  $\sim 20$  K suppression of the glass transition temperature at the surface. The enhancement in surface dynamics is suppressed by coating the metallic glass with a thin layer of amorphous carbon. Parallel molecular dynamics simulations on Ni<sub>80</sub>P<sub>20</sub> show a similar temperature suppression of the surface glass transition temperature and that the enhanced surface dynamics are arrested by a capping layer that chemically binds to the glass surface. Mobility in the near-surface region occurs *via* atomic caging and hopping, with a strong correlation between slow dynamics and high cage-breaking barriers and string-like cooperative motion. Surface and bulk dynamics collapse together as a function of temperature rescaled by their respective glass transition temperatures.

## KEYWORDS

metallic glass, surface dynamics, electron correlation microscopy, molecular dynamics simulations, transport mechanisms

Surface dynamics, the motion of atoms or molecules at or near surfaces of materials, play a large role in materials synthesis, especially for low-dimensional objects like thin films and nanostructures, in processes like crystal growth<sup>1-3</sup> and microfabrication,<sup>4,5</sup> and in various materials properties such as friction,<sup>6</sup> catalysis,<sup>7</sup> sintering,<sup>8</sup> viscosity,<sup>9</sup> and deformation.<sup>10</sup> Mobility of crystal surfaces is often understood in terms of isolated adatoms, hopping across a surface, encountering different morphologies like steps or vacancies with different bonding environments. Mobility of glass surfaces is quite different. Experiments on molecular glasses have consistently shown that all of the molecules in the entire surface layer are highly mobile,<sup>11,12</sup> suggesting collective rearrangements more like those in a bulk liquid than surface hopping. Those collective rearrangements enable surface equilibration to create ultrastable molecular glass thin films<sup>13-15</sup> and unusual surface crystallization kinetics in normal molecular glasses.<sup>16</sup> Similar behavior has been deduced for polymers,<sup>17,18</sup> molecular glasses,<sup>19</sup> and simulated polymer glasses with Lennard-Jones interactions<sup>20,21</sup> from the reduction of the glass transition temperature,  $T_g$ , for very thin films. Models to explain dynamics in such films often employ a two-layer picture<sup>17</sup> consisting of a bulk and an interfacial layer and suggest that dynamics close to the surface and the bulk are quite similar.<sup>19</sup>

Metallic glasses also have fast surfaces. Surface diffusivities near  $T_g$  are high enough to be near liquid-like,<sup>1</sup> which promotes the growth of plate shaped crystals near the surface<sup>22</sup> and very fast motion of metallic glass nanoparticles across a substrate.<sup>23</sup> Metallic glasses also have fast surfaces in molecular dynamics (MD) simulations.<sup>24</sup> Fast surface dynamics persist above the bulk glass transition temperature,  $T_{g,v}$ , into the supercooled liquid state, as shown for metallic glass nanowires using electron correlation microscopy (ECM) experiments.<sup>25</sup> Fast metallic glass

surfaces influence phenomena like crystal nucleation,<sup>25–27</sup> superplastic forming<sup>28</sup> and growth of nanostructures,<sup>22,29</sup> surface friction,<sup>6</sup> and growth of enhanced stability metallic glass thin films.<sup>30,31</sup>

Here, we report ECM experiments studying the fast surface layers of  $\text{Pt}_{57.5}\text{Cu}_{14.7}\text{Ni}_{5.3}\text{P}_{22.5}$  nanowires. Experiments show that the surface glass transition temperature,  $T_{g,s}$ , is suppressed by  $\sim 20$  K with respect to the bulk, and that the dynamics within the surface layer are spatially heterogeneous at a length scale of  $< 1$  nm. Coating the nanowires with amorphous carbon suppresses the fast surface layer, suggesting that decreased coordination at the surface is essential for high mobility. Molecular dynamics simulations on  $\text{Ni}_{80}\text{P}_{20}$  reiterate these findings, confirming the role of decreased coordination at the surface, showing that the motion of atoms in the near-surface layer is quite similar to the bulk supercooled liquid if both are rescaled by their respective  $T_g$ 's, and showing atoms at the surface have shorter relaxation times, experience lower cage-breaking barriers to motion, and are less likely to show string-like cooperative motion.

## RESULTS AND DISCUSSION

Metallic glass nanowires show a near-surface layer that has an order of magnitude faster relaxation dynamics than the bulk at the same temperature. Figs 1(A) and (B) show spatial maps of relaxation time,  $\tau$ , in nanowires heated to 500 K ( $T_{g,v} - 7$  K). The fast surface layer is visible along the edge of the wire in both images. Figs 1(A) was acquired at 0.7 nm spatial resolution, and Fig 1(B) was acquired at 0.23 nm. The map in (B) has a smaller speckle size, consistent with its higher resolution. Both images show a thickness of the surface layer of  $\sim 1$  nm, indicating that 1 nm is the physical thickness, not limited by experimental resolution. 1 nm thickness means the fast surface layer involves approximately three monolayers, so we are not observing adatom surface hopping as occurs on the surface of a crystal. This result is consistent with recent simulation results on metallic glass surface mechanisms which also demonstrated that the mechanism was not

adatoms.<sup>32</sup> The higher resolution map shows that the dynamics inside the surface layer are noticeably spatially heterogeneous. At all temperatures, the histogram of near surface relaxation times is well described by a log-normal distribution, characteristic of a random, non-negative process, and the stretching exponent  $\beta$  varies from 0.06 to 1 (supplementary figure 1). There are no clear trends in the distributions of either  $\tau$  or  $\beta$  as a function of temperature over the limited range studied here. Averaged, normalized profiles of surface dynamics as a function of distance from the surface are shown in supplementary figure 4. From supplementary fig 4(b), there is no clear trend with temperature in layer thickness or the dependence of  $\tau$  with distance from the surface over the small range of temperature accessible to these experiments.

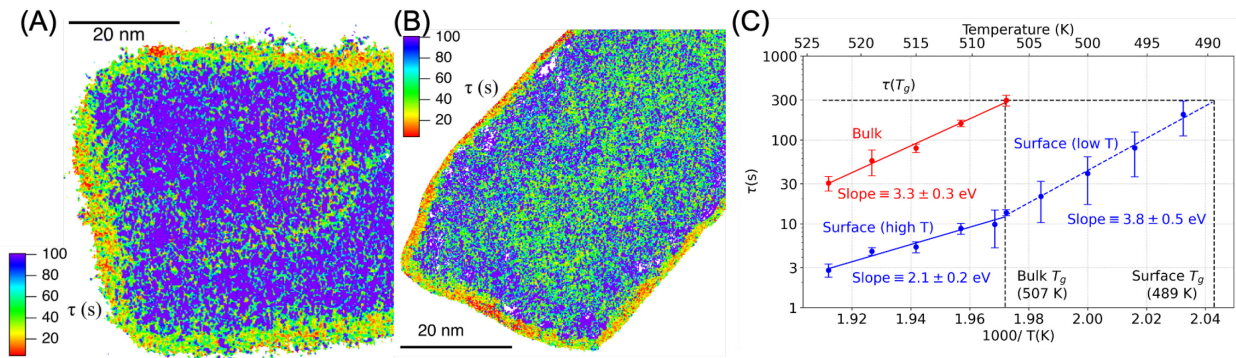


**Fig 1:** (A) and (B) Relaxation time ( $\tau$ ) map of a nanowire heated *in situ* to 500 K showing a near-surface layer with faster relaxation dynamics compared to the bulk. (A) was acquired at 0.7 nm spatial resolution and (B) was acquired at 0.23 nm, as shown by the smaller features. (C) The mean structural relaxation time for the nanowire interior (bulk) and the near-surface layer. The error bars are the standard deviation of the measured relaxation time at different positions. Fitting to the Arrhenius form yields activation energies of  $3.3 \pm 0.3$  eV for the bulk (linear fit Pearson's  $R = 0.98$ ),  $2.1 \pm 0.2$  eV for the near-surface layer above  $T_{g,v}$  (linear fit Pearson's  $R = 0.92$ ), and  $3.8 \pm 0.5$  eV below  $T_{g,v}$  (linear fit Pearson's  $R = 0.97$ ). Fitting all the surface data with a single linear fit yields a poor linear fit with Pearson's  $R = 0.71$ , so that fit is not used to estimate a single activation energy for the near-surface layer. The near-surface layer glass transition temperature is suppressed by 18 K compared to the bulk. Data for the bulk are reproduced from Ref. 25. Activation energies reported here for previously published data from ref. 25 are revised due to improved treatment of experimental uncertainties.

Fig 1 (C) shows average relaxation times in the near surface layer of the nanowires as a function of temperature. Bulk data from Ref. <sup>25</sup> are reproduced for comparison. (At the

temperatures studied here, bulk relaxation times are too long to obtain good convergence in ECM experiments.<sup>33)</sup> At  $T_g$  for the nanowires determined by calorimetry (507 K), the average bulk relaxation time is 297 s and the average surface relaxation time is 14 s. The surface continues to slow as the temperature drops. Extrapolating the surface relaxation time below  $T_{g,v}$  with an Arrhenius form (valid over small temperature ranges) to the bulk relaxation time at  $T_{g,v}$  reveals a  $T_{g,s}$  of 489 K, 18 K lower than the bulk. STEM EDS mapping performed on a nanowire annealed at 492 K for 3 hours shows no evidence of surface segregation (supplementary figure 2). Fitting to the Arrhenius form yields activation energies of  $3.3 \pm 0.3$  eV for the bulk,  $2.1 \pm 0.2$  eV for the near-surface layer above  $T_{g,v}$ , and  $3.8 \pm 0.5$  eV below  $T_{g,v}$ .

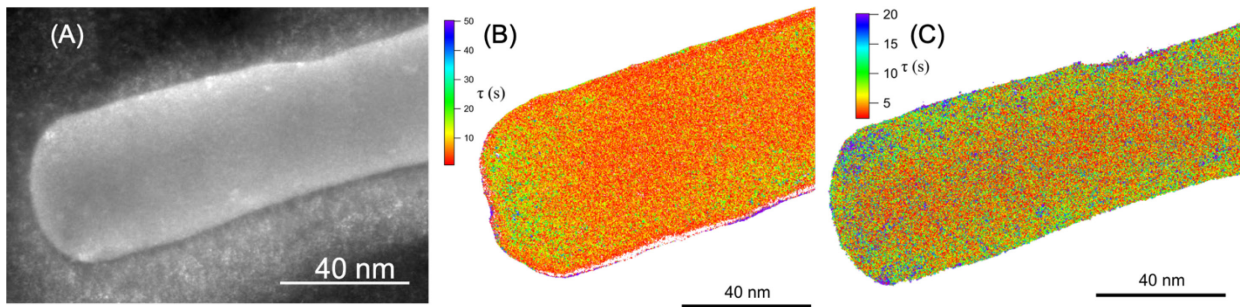


**Fig 2:** (A) Static, room-temperature DF TEM image showing a nanowire coated with amorphous carbon, (b-c) Relaxation time maps of amorphous carbon coated nanowires heated *in situ* to (B) 515 K and (C) 519 K. The fast near-surface layer is suppressed. This result indicates that access to the open volume available at the surface is responsible for the enhanced mobility, since removing access to it suppresses the fast surface layer.

Fig 2 shows the effect of a surface confinement layer on relaxation dynamics in nanowires coated with a  $\sim 10$  nm layer of amorphous carbon. Fig 2(A) shows a static dark-field TEM image at room temperature of a nanowire coated with amorphous carbon. The carbon is thicker near the wire, and thus visible in the image, due to shadowing effects during deposition. Figs 2(B) and (C) show relaxation time maps in amorphous carbon coated nanowires heated *in situ* at 515 K and 519 K respectively. At 519 K, the fast near-surface layer is not observed. At 515 K, there may be some indication of enhanced surface dynamics, but we attribute this layer to difficulty in locating the

precise surface of the nanowire amidst the contrast from the carbon coating. If the layer is there, it is suppressed, since it is both thinner and closer in dynamics to the bulk than without the layer. Averaged profile of surface dynamics as a function of distance from the surface is shown in supplementary figure 4(b) for the nanowire heated at 519 K. The near surface layer has significantly slower dynamics compared to the bulk.

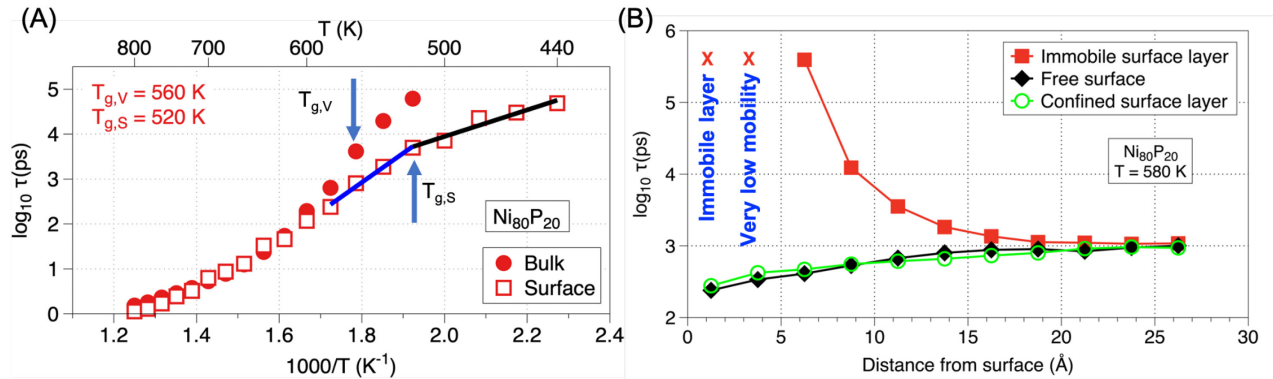


**Fig 3:** (A) Structural relaxation time as a function of temperature for the bulk and the surface layer calculated from MD simulations. The glass transition temperature for the surface layer, determined from the change of slope, is 40 K lower than the bulk glass transition temperature for this system. (B) Structural relaxation time measured at 580 K as a function of distance from the surface for a free surface, with the first layer held stationary, and with a physical surface confinement imposed by using reflective boundary conditions. Keeping the top layer stationary renders the second layer from the surface almost immobile. Physically confining the surface increases the relaxation time of the surface layer only slightly (by  $\sim 16\%$ ) compared to free surface.

To simulate surface kinetics for comparison to  $Pt_{57.5}Cu_{14.7}Ni_{5.3}P_{22.5}$  we carried out molecular dynamics simulations on  $Ni_{80}P_{20}$ , as no interatomic potential for the  $Pt_{57.5}Cu_{14.7}Ni_{5.3}P_{22.5}$  quaternary is available. The  $Ni_{80}P_{20}$  alloy allowed us to use an interatomic potential with well-established glass properties and mimicked the metal-metalloid character of the original composition. Fig 3(A) shows structural relaxation times as a function of temperature for the bulk and surface monolayer. The  $T_{g,s}$  measured from the change in slope of  $\tau$  is 520 K, which is 40 K lower than the  $T_{g,v}$  measured from the change in slope of energy (or volume) *versus* temperature during quenching. Fig 3(B) shows the structural relaxation time at 580 K, well above both  $T_g$ 's, as

a function of distance from the surface, monolayer by monolayer (each monolayer defined as 2.5 Å), for the system with a free surface, for a system in which the first monolayer of the liquid is artificially held stationary in the simulation, and for a system where the surface layer is physically confined without chemical bonds by imposing reflective boundary conditions. The free surface relaxation time converges to the bulk value over 6 monolayers, or about 1.5 nm. With the immobile surface, the second monolayer is also rendered almost immobile, with a relaxation time too large to be reliably measured in the duration of the simulations. Layers 3-9 converge to the (faster) bulk relaxation time over a distance of 1.5 nm. For the system with the physically confined surface, the relaxation times are very similar to that observed with a free surface. The outer monolayer has slightly higher relaxation time (by  $\sim 16\%$ ) than a free surface monolayer, as expected.

A depth profile of composition of P atoms shows surface segregation (supplementary figure 3), with a P-rich surface layer having a composition around  $\text{Ni}_{67.5}\text{P}_{32.5}$ , followed by two monolayers with P content lower than the bulk content. By a depth of 1 nm, the P content has converged to the bulk value. In MD simulations, the  $T_{g,v}$  of this P-rich composition is 440 K, which is 120 K lower than the  $T_{g,v}$  of  $\text{Ni}_{80}\text{P}_{20}$ , revealing that the difference in dynamics between the surface layer and the bulk has at least a contribution other than surface segregation.

Fig. 4 shows that the surface dynamics behave in many ways like the bulk dynamics at a higher temperature. The relaxation time, the atomic jump rate, and the percentage of atoms engaged in string-like cooperative motion as a function of temperature provide atomic-level insight into the supercooled liquid behavior. Fig 4 (A) shows the relaxation time as a function of temperature normalized by their respective  $T_g$ 's for bulk  $\text{Ni}_{80}\text{P}_{20}$ , its free surface layer, and for a bulk glass with the surface composition,  $\text{Ni}_{67.5}\text{P}_{32.5}$ . The absolute relaxation times at each normalized temperature are quite similar for the  $\text{Ni}_{80}\text{P}_{20}$  surface layer and bulk. The slope of the

bulk relaxation time as  $T_g/T$  approaches one is higher than the surface relaxation time slope, which indicates different fragility. However, the slope of the bulk  $\text{Ni}_{67.5}\text{P}_{32.5}$  relaxation time is the same as the  $\text{Ni}_{80}\text{P}_{20}$  surface, indicating that the difference in fragility is likely caused by the change in composition, not solely the presence of the surface. Indeed, the  $\text{Ni}_{80}\text{P}_{20}$  surface and the same composition  $\text{Ni}_{67.5}\text{P}_{32.5}$  bulk have the same relaxation times over the entire range of normalized temperature.

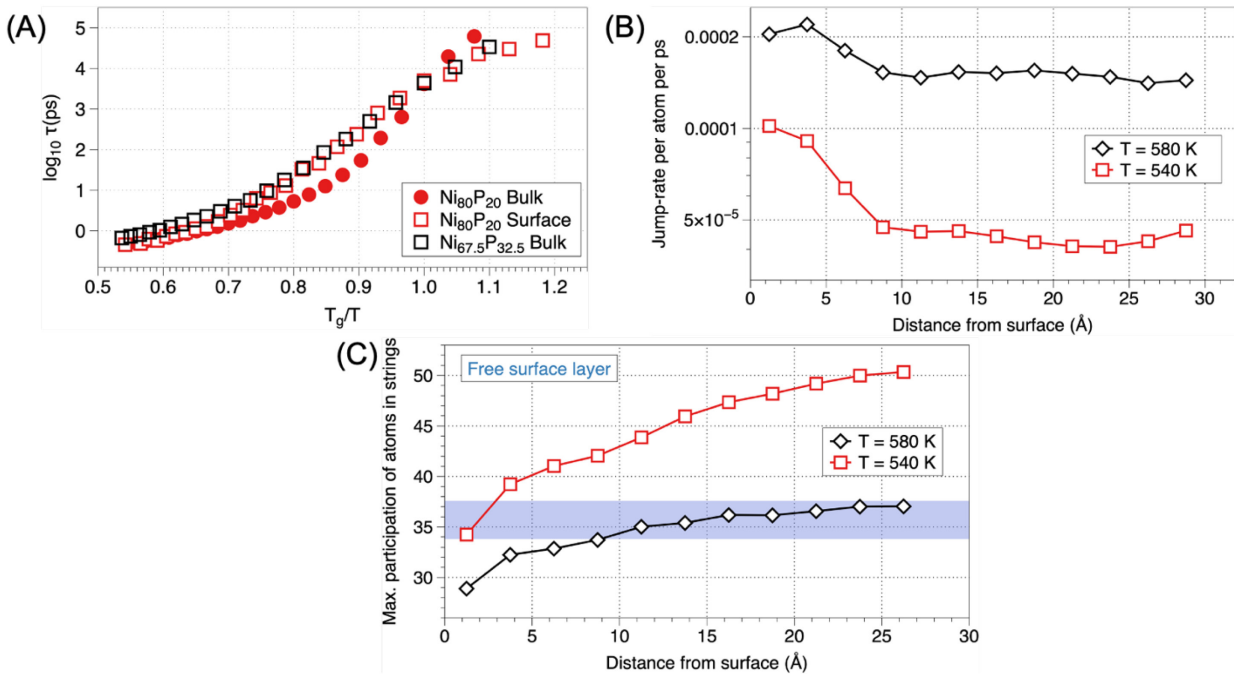


**Fig 4:** For the  $\text{Ni}_{80}\text{P}_{20}$  system with a free surface, (A) variation of surface and bulk relaxation times ( $\tau$ ) as a function of temperature scaled to  $T_{g,s}$  and  $T_{g,v}$  respectively. The bulk relaxation time of  $\text{Ni}_{67.5}\text{P}_{32.5}$  is also shown. (B) The jump rate of atoms as a function of distance from surface at 540 K and 580 K. The jump rate of atoms for the surface atoms at 540 K is similar to the jump rate of atoms for the bulk at 580 K. (C) The participation of atoms in strings as a function of distance from surface at 540 K and 580 K. The participation of atoms in strings for the surface atoms at 540 K is similar to the fraction of atoms in strings for the bulk at 580 K as highlighted by the shaded area.

Fig 4 (B) shows the atomic jump-rate as a function of distance from the free surface at 540 K and 580 K for  $\text{Ni}_{80}\text{P}_{20}$ . Atomic jump-rate is a measure of cage-breaking barrier to atomic mobility. At both temperatures, the jump-rate decreases as we go deeper into the bulk and away from the free surface, indicating that the cage-breaking barriers are low near the surface and

increase as we approach the bulk. The jump-rate for the surface at 540 K is similar to the rate in the bulk at 580 K, indicating that the free surface behaves like the bulk supercooled liquid at a higher temperature.

Fig 4 (C) shows the percentage of atoms engaged in string-like cooperative motion in each layer at 540 K and 580 K starting from the free surface. The percentage of atoms engaged in string-like motion varies with the time scale for the motion. At short timescales, ballistic motion dominates, and the string-like percentage is small. At long timescales, diffusive motion dominates<sup>34</sup> and the string-like percentage is again small. The string-like percentage peaks at an intermediate timescale which varies for each layer of atoms, since they have different structural relaxation times. We use the peak of string-like percentage as a function of timescale for motion as a metric for comparison of propensity of string-like motion for atoms in different layers of the glass. At both 540 K and 580 K, the percentage of atoms engaged in string-like cooperative motion increases as we go into the bulk of the sample starting from the free surface. The percentage of atoms engaged in string-like motion at the surface at 540 K is similar to the percentage in the bulk at 580 K as highlighted by the shaded area, again indicating similar behavior for the surface and the bulk at a higher temperature.

Fig 5 shows results from simulations on the  $\text{Ni}_{80}\text{P}_{20}$  system with an immobile surface performed at 580 K. Fig 5 (A) shows the atomic jump-rate and jump-length as a function of distance from the surface, normalized to the bulk value. The jump-rate, which is a measure of the atomic cage-breaking barriers, decreases significantly as we approach the immobile layer. Combined with our observations in Fig 4 (B), the atomic jump rate is higher in the free surface, and lower close to the immobile layer, when compared to the bulk. The jump-rate is related to the cage-breaking barrier experienced by atoms, so the local cage-breaking barrier plays a key role in

influencing the mobility and relaxation dynamics. The jump length does not vary as significantly from the surface to the bulk, so changes in this length do not play a significant role in the changes in mobility. Caging and hopping behavior in near-surface layers has been investigated in greater detail elsewhere.<sup>32</sup>

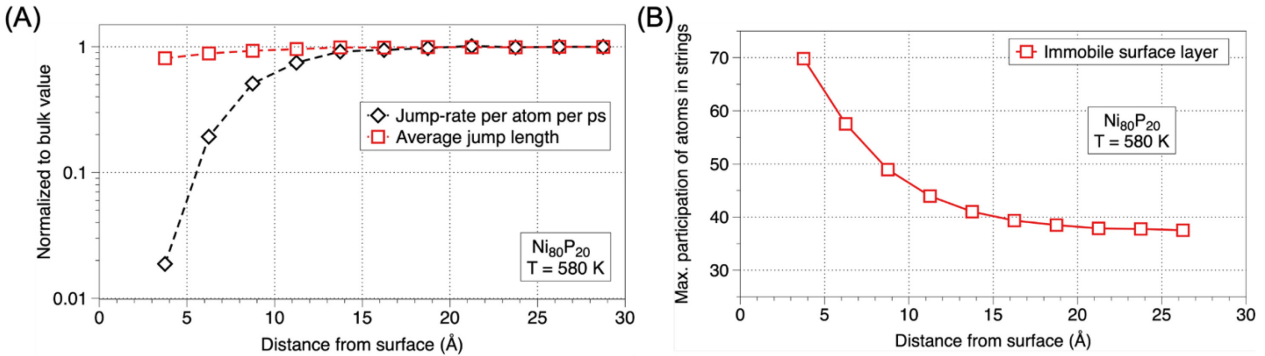


**Fig 5:** (A) The variation of jump-rate and jump-length as a function of distance from surface for the Ni<sub>80</sub>P<sub>20</sub> system with an immobile surface. Low mobility close to the top immobile layer is mainly attributed to a high cage-breaking barrier deduced from low jump rate. (B) The participation of atoms in strings as a function of distance from surface for the Ni<sub>80</sub>P<sub>20</sub> system with an immobile surface

Fig 5 (B) shows the maximum participation of atoms in strings as a function of distance from the surface with an immobile surface layer. With an immobile layer, the participation in string-like motion is very high close to the immobile surface and converges to the bulk value that we saw in the system with a free surface in 5-6 layers (1.25-1.5 nm). With the immobile surface layer, the relaxation behavior and mobility both have a steep gradient from the surface to the bulk.

Taken together, the experimental and simulation results demonstrate that, for the systems studied, the near-surface region of a metallic glass with a free surface behaves at temperatures below  $T_{g,v}$  but above  $T_{g,s}$  like a normal, albeit supercooled liquid. The experiments show that fast dynamics persist approximately 20 K below the  $T_{g,v}$  in ~1 nm thick layer. Simulations agree with this basic phenomenology, although the gap in  $T_{g,s}$  and  $T_{g,v}$  is 40 K. Simulations also help validate

our experimental approach to measuring  $T_{g,s}$ , as Fig 3 (A) shows that the relaxation time values are similar for the bulk and the surface layer at their respective  $T_g$ 's. Overall, although our experiments and simulations were performed on different systems, with cooling rates that differ by 7-8 orders of magnitude leading to drastically different thermal histories, there is a high degree of agreement in the observed phenomena. These similarities support the hypothesis that these features of metallic glass surface dynamics may be quite general across many different metallic glass alloys, cooling rates, and ageing histories. Experiments show that the dynamics in the surface layer are spatially heterogenous, with similar distributions of relaxation time and stretching exponents to bulk dynamics. Simulations show that even the atomistic details of relaxation time, cage breaking barrier, and propensity for cooperative motion are quite similar in the near-surface layer compared to the bulk liquid at a higher temperature.

These observations are consistent with previous experimental and simulation reports of high mobility in the surface layer of metallic glasses near the  $T_{g,v}$ ,<sup>1,23,35</sup> which is similar to the picture of a liquid surface that persists below the  $T_{g,v}$  that has been extensively developed for molecular and polymeric glasses.<sup>16,17,36-38</sup> Our results expand upon this picture by adding metallic glasses to the materials exhibiting these phenomena, directly measuring the surface layer thickness, and demonstrating spatial heterogeneity. We also introduce the idea of and measure  $T_{g,s}$ , the temperature at which the surface falls out of equilibrium and becomes glassy. In particular, our observations suggest that the dynamics of supercooled metallic glass systems can be modelled by a two-layer approach where the bulk and the near-surface layer are very similar but shifted in temperature, represented in their respective glass transition temperatures. This is also supported by our experimental observations as the activation energies for the near-surface layer below  $T_{g,v}$  and the bulk above  $T_{g,v}$  are in agreement (with uncertainties) as shown in fig 1(C). This observation

is similar to experimental reports on polymer glasses where glassy dynamics is described as a combination of the bulk and a mobile surface having faster dynamics and a fixed thickness.<sup>17</sup> We have not observed any temperature dependence of the thickness of the near-surface layer within the (admittedly small) temperature range of our experiments. Our results may imply that the near-surface layer is thick enough to have “bulk-like” atomic motions. In experiments, the surface and bulk have qualitatively similar correlation lengths for spatially heterogeneous dynamics.

Our observations also identify the origin of short relaxation times near the surface: it arises due to reduced coordination making it easier for atoms to break their cages and diffuse in the plane. If we impose barriers to atomic hopping with chemical interactions with the liquid, either by carbon coating in experiments or by an immobile surface layer in simulations, the fast near-surface layer is suppressed. However, if we physically confine the surface layer without chemical interactions by imposing reflective boundary conditions, there is very little change to atomic mobility. This shows that a physical barrier alone does suppress fast surface dynamics, which is consistent with our previous work<sup>32</sup> demonstrating that adatom diffusion is not significant in metallic glass surface diffusion. A chemical bond between the metallic glass surface atoms and the carbon coating imposes a significant barrier to atomic hopping, which decreases atomic mobility. The capping layer removes the similarity between the surface and the higher-temperature bulk we observe with the free surface. In simulations with a stationary surface layer, the near surface layer dynamics become even slower than bulk dynamics. The capping layer introduces large gradients in relaxation time, cage-breaking barriers, and propensity for string like cooperative motion. However, a correlation remains between decreased atomic mobility and increased propensity for string-like cooperative motion, as shown in Fig 5. This correlation has been seen previously in other systems<sup>17,35</sup> and suggests that atoms in regions with reduced access to open volume and

stronger cage-breaking barriers are more likely to move in a cooperative string-like fashion. We speculate that the strength of the bonding between the capping layer and the liquid surface might influence the extent of slowdown of dynamics, but we have not tested this hypothesis.

Beyond fundamental scientific interest, a better understanding of metallic glass surface mobility and how it can be controlled will guide synthesis and use of metallic glasses. A nanometer-thick, highly mobile surface layer bodes well for efforts to deposit ultrastable metallic glass thin films,<sup>31,39</sup> since high mobility may allow the near-surface atoms to find low enthalpy configurations without bulk crystallization. It may also play a role in superplastic forming of nanostructures like the nanowires we have studied here, which are processed near the  $T_{g,v}$ . Surface diffusion has been recently shown to play a large role in pressure-induced forming of crystalline nanowires.<sup>29</sup> High surface mobility may also influence friction of metallic glasses in service near  $T_g$ .<sup>6,40-42</sup> Control of surface mobility using a capping layer that remains immobile at service temperatures could help avoid undesirable effects like nucleation of surface crystals by suppressing surface layer mobility, and the observed behavior near the immobile layer points to an interesting research direction as interface behavior in confined liquids is of importance for various classes of glassy materials which are used in microfabrication and battery technology.

## CONCLUSIONS

In summary, we have shown in both sub-nanometer resolution experiments and atomistically-resolved simulations that metallic glasses have a surface layer  $\sim 1$  nm thick with faster dynamics than the bulk. This layer remains liquid, with a short mean structural relaxation time, well below the bulk glass transition temperature, until it cools below the surface glass transition temperature, which is tens of Kelvins below the bulk glass transition temperature. If the

surface and bulk dynamics are rescaled by their respective glass transition temperatures, they exhibit very similar behavior. Simulations show that the two regions have the same kind of caging and hopping behavior and the same degree of cooperative motion. Experiments show that both surface and bulk have dynamics that are spatially heterogeneous at the nanometer scale. Both experiments and simulations show that the origin of the fast near-surface layer is the reduced coordination at the surface. If a capping layer that chemically binds to the surface atoms is introduced, the fast surface layer is suppressed. These findings have implications for a wide variety of metallic glass syntheses and properties involving surfaces, including growth of ultrastable films, fabrication of nanostructures by superplastic forming, surface crystallization, and friction at small length scales.

## MATERIALS AND METHODS

### Nanowire synthesis and ECM sample preparation

We fabricated  $\text{Pt}_{57.5}\text{Cu}_{14.7}\text{Ni}_{5.3}\text{P}_{22.5}$  nanowires with a diameter of  $\sim 40$  nm by nanomoulding as described in detail elsewhere.<sup>43</sup> As-fabricated nanowires were attached to a substrate plate of the same bulk metallic glass. The bulk metallic glass plate was rinsed with distilled water and isopropyl alcohol to minimize the residual salts and anodized aluminum oxide from fabrication. Then the plate was immersed in methanol and nanowires were released from the substrate by sonication for 15–20 min. The nanowires immersed in methanol were dropped on to a DENSSolutions Wildfire TEM heating chip using a micropipette (1.5–1.8  $\mu\text{L}$ ). Upon evaporation of methanol, some nanowires were randomly attached to the 90% electron transparent  $\text{SiN}_x$  membrane present on windows in the chip. We drop 10–12 drops of the nanowire suspension in methanol, on to the heating chip allowing 5 min methanol evaporation time between drops to

achieve a uniform distribution of isolated nanowires. We plasma cleaned the sample for 10 mins in a 20 psi Ar + O<sub>2</sub> mixture to remove organic contaminants which may be introduced from the methanol. Nominally 10 nm thick amorphous carbon was sputtered onto some of the nanowire coated heating chips after blocking out the electrical contact pads with tape using a Leica EM 600 coating system with a carbon thread deposition head.

### ECM experiment and data analysis

The heating chips were loaded on to a DENSsolutions SH30 single-tilt heating holder, which can provide temperature stability of 0.05 K and temperature accuracy of 0.5%. Data was acquired at 508 K ( $\sim T_{g,v}$ ), 504 K, 500 K, 496 K, and 492 K. Due to the slower kinetics, the experiments on amorphous carbon coated nanowires were performed at 515 K and 519 K. The samples were heated to the target temperature at a rate of 20 K/min and equilibrated for at least five times the measured structural relaxation time shown in Fig. 1(C).

ECM measurements were carried out using tilted dark-field TEM imaging. Experiments used the University of Wisconsin-Madison FEI Titan with probe aberration corrector at 200 kV, operated in TEM mode. An objective aperture of 10  $\mu\text{m}$  in diameter or 2.83 mrad half angle was inserted for low resolution experiments, giving rise to speckles in the image  $\sim 0.7$  nm in diameter, calculated from the Rayleigh criterion and confirmed by imaging. The speckle size sets the spatial resolution of the ECM experiment. For the low resolution experiments, an Orius 2.6 x 4 k fast CCD with 1 ms readout time was used to record the time series 256 by 256 pixel images with a pixel size of 0.25 nm. Higher resolution ECM measurements were performed using an objective aperture of 30  $\mu\text{m}$  diameter, yielding a resolution of  $\sim 0.23$  nm in diameter. For these

measurements, a fast DE-16 direct electron camera was used with a hardware binning by a factor of 2 to record 2k by 2k pixel images at a pixel size of 0.08 nm.

The interval between frames in the image series was set as a function of temperature to meet the sampling requirements for ECM.<sup>33</sup> The acquisition rate was set to 10, 4, 2, 1 and 1 fps for temperatures 508, 504, 500, 496, and 492 K respectively. Every image series consists of ~4000 frames. Rigid image registration with the Pystackreg<sup>44</sup> package was used to perform two-step drift correction with single-pixel accuracy on the image series. First each frame was aligned with respect to its previous frame to remove local misalignments, and then each frame was aligned with respect to the first frame in the series to remove global misalignments. Spatial maps of relaxation time ( $\tau$ ) and stretching exponent ( $\beta$ ) were extracted by calculating the time autocorrelation function,  $g_2(t)$ , and by fitting it to a Kohlrausch-Williams-Watts (KWW) stretched exponential form for every pixel. The analysis has been described in detail elsewhere.<sup>25</sup>

## MD simulations

Molecular dynamics (MD) simulations were applied to study a Ni<sub>80</sub>P<sub>20</sub> model metallic glass using the Sheng *et al.* embedded atom method potential<sup>45</sup> in LAMMPS.<sup>46</sup> A cubic simulation cell of 16384 atoms was initially equilibrated at 1500 K for 2 ns and then quenched to 1000 K in 50 K decrements at the rate of 100 K per 6 ns. The system was subsequently cooled in 20 K intervals at the rate of 100 K per 60 ns, corresponding to a quench rate of  $\sim 10^9$  K/s. We used the NPT ensemble and periodic boundary conditions (PBC) during the quenching process. Then, the simulation cell boundaries were extended 10 Å along the  $\pm z$ -axis, creating free surfaces and vacuum. To study the dynamics at a given temperature, the NVT ensemble and PBC were applied and the system was initially equilibrated for 1 ns to make sure the newly created surfaces at the two edges are

relaxed before data were collected. Atoms in the outer 2.5 Å of the sample along the  $\pm z$ -axis (or 12.5 Å of the cell considering the empty space), which is the size of a monolayer as determined from radial distribution function of atoms, were used to evaluate the properties associated with the surface. Relaxation times are calculated from the decay of the intermediate scattering function.<sup>47</sup> Time dependent properties of atoms in a layer make use of data from two times and were determined for atoms belonging to the layer at both times.

## ACKNOWLEDGMENTS

**FUNDING:** We acknowledge support for this research from the U. S. National Science Foundation through the Wisconsin MRSEC (DMR-1720415) and DMR-1807241. DMR-1720415 supported simulation studies by A. A. and D. M. and facilities for electron microscopy experiments. DMR-1807241 supported electron microscopy experiments by D. C. and P. M. V. Nanowires synthesis by J. K. and J. S. was supported by the U.S. Department of Energy through the Office of Science, Basic Energy Sciences, Materials Science and Engineering Division (No. DE SC0004889). A. A. and D. M. also acknowledge the Extreme Science and Engineering Discovery Environment (XSEDE), which is supported by National Science Foundation grant number OCI-1053575, and the Center for High Throughput Computing at UW-Madison for the computing resources.

**AUTHOR CONTRIBUTIONS:** D. C. and P. M. V. conceived the study and designed and performed ECM and STEM EDS experiments and related data analysis. A. A. and D. M. performed MD simulations and related data analysis. J. K. and J. S. performed synthesis of  $\text{Pt}_{57.5}\text{Cu}_{14.7}\text{Ni}_{5.3}\text{P}_{22.5}$  nanowires. All the authors contributed to the discussion and interpretation of the results. D. C. and P. M. V. wrote the manuscript, which all authors revised and approved.

## ASSOCIATED CONTENT

FINANCIAL INTERESTS: The authors declare no competing financial interests.

DATA AND MATERIALS AVAILABILITY: All data used in this work is available *via* the Materials Data Facility, <https://doi.org/10.18126/cvrk-0hdg>.

SUPPLEMENTARY INFORMATION: A document with supplementary figures containing further detail to results mentioned in the main text is available free of charge online.

- Figure S1: Distributions of near-surface  $\tau$  and  $\beta$  values at different temperatures
- Figure S2: STEM-EDS mapping of a  $\text{Pt}_{57.5}\text{Cu}_{14.7}\text{Ni}_{5.3}\text{P}_{22.5}$  nanowire to investigate composition segregation during *in situ* experiments
- Figure S3: Composition profile of P atoms in the simulated  $\text{Ni}_{80}\text{P}_{20}$  system to investigate composition segregation during MD simulations
- Figure S4: Average normalized depth profile of  $\tau$  for uncoated and amorphous carbon nanowires to investigate thickness of the near-surface layer where the dynamics are strongly influenced by interface bonds

## REFERENCES

- (1) Cao, C. R.; Lu, Y. M.; Bai, H. Y.; Wang, W. H. High Surface Mobility and Fast Surface Enhanced Crystallization of Metallic Glass. *Appl. Phys. Lett.* **2015**, *107* (14), 8–12. <https://doi.org/10.1063/1.4933036>.
- (2) Chookajorn, T.; Murdoch, H. A.; Schuh, C. A. Design of Stable Nanocrystalline Alloys. *Science* (80-. ). **2012**, *337* (6097), 951–954. <https://doi.org/10.1126/science.1224737>.
- (3) Liu, Z.; Han, G.; Sohn, S.; Liu, N.; Schroers, J. Nanomolding of Crystalline Metals: The Smaller the Easier. *Phys. Rev. Lett.* **2019**.

- <https://doi.org/10.1103/PhysRevLett.122.036101>.
- (4) Sun, J.; He, L.; Lo, Y.-C.; Xu, T.; Bi, H.; Sun, L.; Zhang, Z.; Mao, S. X.; Li, J. Liquid-like Pseudoelasticity of Sub-10-Nm Crystalline Silver Particles. *Nat. Mater.* **2014**.  
<https://doi.org/10.1038/nmat4105>.
- (5) Delcambre, S. P.; Riggleman, R. A.; De Pablo, J. J.; Nealey, P. F. Mechanical Properties of Antiplasticized Polymer Nanostructures. *Soft Matter* **2010**.  
<https://doi.org/10.1039/b926843j>.
- (6) Rahaman, M. L.; Zhang, L. C.; Ruan, H. H. Understanding the Friction and Wear Mechanisms of Bulk Metallic Glass under Contact Sliding. *Wear* **2013**, *304* (1–2), 43–48.  
<https://doi.org/10.1016/j.wear.2013.04.022>.
- (7) Wang, J. Q.; Liu, Y. H.; Chen, M. W.; Xie, G. Q.; Louzguine-Luzgin, D. V.; Inoue, A.; Perepezko, J. H. Rapid Degradation of Azo Dye by Fe-Based Metallic Glass Powder. *Adv. Funct. Mater.* **2012**. <https://doi.org/10.1002/adfm.201103015>.
- (8) Prado, M. O.; Zanotto, E. D. Glass Sintering with Concurrent Crystallization. *Comptes Rendus Chim.* **2002**. [https://doi.org/10.1016/S1631-0748\(02\)01447-9](https://doi.org/10.1016/S1631-0748(02)01447-9).
- (9) Zhang, Y.; Glor, E. C.; Li, M.; Liu, T.; Wahid, K.; Zhang, W.; Riggleman, R. A.; Fakhraai, Z. Long-Range Correlated Dynamics in Ultra-Thin Molecular Glass Films. *J. Chem. Phys.* **2016**. <https://doi.org/10.1063/1.4962734>.
- (10) Nieh, T. G.; Yang, Y.; Lu, J.; Liu, C. T. Effect of Surface Modifications on Shear Banding and Plasticity in Metallic Glasses: An Overview. *Progress in Natural Science: Materials International*. 2012. <https://doi.org/10.1016/j.pnsc.2012.09.006>.
- (11) Zhu, L.; Brian, C. W.; Swallen, S. F.; Straus, P. T.; Ediger, M. D.; Yu, L. Surface Self-Diffusion of an Organic Glass. *Phys. Rev. Lett.* **2011**.

<https://doi.org/10.1103/PhysRevLett.106.256103>.

- (12) Daley, C. R.; Fakhraai, Z.; Ediger, M. D.; Forrest, J. A. Comparing Surface and Bulk Flow of a Molecular Glass Former. *Soft Matter* **2012**.  
<https://doi.org/10.1039/c2sm06826e>.
- (13) Swallen, S. F.; Kearns, K.; Mapes, M.; Kim, Y. S.; McMahon, R. J.; Ediger, M. D.; Wu, T.; Yu, L.; Satija, S. Organic Glasses with Exceptional Thermodynamic and Kinetic Stability. *Science (80-. )*. **2007**, *315* (January), 353–356.
- (14) Singh, S.; Ediger, M. D.; De Pablo, J. J. Ultrastable Glasses from in Silico Vapour Deposition. *Nat. Mater.* **2013**. <https://doi.org/10.1038/nmat3521>.
- (15) Lyubimov, I.; Ediger, M. D.; De Pablo, J. J. Model Vapor-Deposited Glasses: Growth Front and Composition Effects. *J. Chem. Phys.* **2013**, *139* (14).  
<https://doi.org/10.1063/1.4823769>.
- (16) Wu, T.; Yu, L. Surface Crystallization of Indomethacin below T<sub>G</sub>. *Pharm. Res.* **2006**.  
<https://doi.org/10.1007/s11095-006-9023-4>.
- (17) Yang, Z.; Fujii, Y.; Lee, F. K.; Lam, C.; Tsui, O. K. C. Glass Transition Dynamics and Surface Layer Mobility in Unentangled Polystyrene Films. *Science (80-. )*. **2010**, *328* (5986), 1676–1679. <https://doi.org/10.1126/science.1184394>.
- (18) Salez, T.; Salez, J.; Dalnoki-Veress, K.; Raphaël, E.; Forrest, J. A. Cooperative Strings and Glassy Interfaces. *Proc. Natl. Acad. Sci.* **2015**.  
<https://doi.org/10.1073/pnas.1503133112>.
- (19) Zhang, Y.; Woods, C. N.; Alvarez, M.; Jin, Y.; Riggleman, R. A.; Fakhraai, Z. Effect of Substrate Interactions on the Glass Transition and Length-Scale of Correlated Dynamics in Ultra-Thin Molecular Glass Films. *J. Chem. Phys.* **2018**, *149* (18).

<https://doi.org/10.1063/1.5038174>.

- (20) Shavit, A.; Riggleman, R. A. Physical Aging, the Local Dynamics of Glass-Forming Polymers under Nanoscale Confinement. *J. Phys. Chem. B* **2014**.  
<https://doi.org/10.1021/jp502952n>.
- (21) Peter, S.; Meyer, H.; Baschnagel, J. Thickness-Dependent Reduction of the Glass-Transition Temperature in Thin Polymer Films with a Free Surface. *J. Polym. Sci. Part B Polym. Phys.* **2006**. <https://doi.org/10.1002/polb.20924>.
- (22) Chen, L.; Cao, C. R.; Shi, J. A.; Lu, Z.; Sun, Y. T.; Luo, P.; Gu, L.; Bai, H. Y.; Pan, M. X.; Wang, W. H. Fast Surface Dynamics of Metallic Glass Enable Superlatticelike Nanostructure Growth. *Phys. Rev. Lett.* **2017**, *118* (1), 1–5.  
<https://doi.org/10.1103/PhysRevLett.118.016101>.
- (23) Cao, C. R.; Huang, K. Q.; Shi, J. A.; Zheng, D. N.; Wang, W. H.; Gu, L.; Bai, H. Y. Liquid-like Behaviours of Metallic Glassy Nanoparticles at Room Temperature. *Nat. Commun.* **2019**, *10* (1). <https://doi.org/10.1038/s41467-019-09895-3>.
- (24) Chen, H.; Qu, B.; Li, D.; Zhou, R.; Zhang, B. Atomic Structure and Dynamics Properties of Cu 50 Zr 50 Films. *J. Appl. Phys.* **2018**, *123* (2), 025307.  
<https://doi.org/10.1063/1.5011122>.
- (25) Zhang, P.; Maldonis, J. J.; Liu, Z.; Schroers, J.; Voyles, P. M. Spatially Heterogeneous Dynamics in a Metallic Glass Forming Liquid Imaged by Electron Correlation Microscopy. *Nat. Commun.* **2018**, *9* (1), 1–7. <https://doi.org/10.1038/s41467-018-03604-2>.
- (26) Kelton, K. F. Crystal Nucleation in Liquids and Glasses. *Solid State Phys. - Adv. Res. Appl.* **1991**. [https://doi.org/10.1016/S0081-1947\(08\)60144-7](https://doi.org/10.1016/S0081-1947(08)60144-7).
- (27) Sohn, S.; Jung, Y.; Xie, Y.; Osuji, C.; Schroers, J.; Cha, J. J. Nanoscale Size Effects in

- Crystallization of Metallic Glass Nanorods. *Nat. Commun.* **2015**.  
<https://doi.org/10.1038/ncomms9157>.
- (28) Chen, Z.; Datye, A.; Ketkaew, J.; Sohn, S.; Zhou, C.; Dagdeviren, O. E.; Schroers, J.; Schwarz, U. D. Relaxation and Crystallization Studied by Observing the Surface Morphology Evolution of Atomically Flat Pt<sub>57.5</sub>Cu<sub>14.7</sub>Ni<sub>5.3</sub>P<sub>22.5</sub> upon Annealing. *Scr. Mater.* **2020**, *182*, 32–37. <https://doi.org/10.1016/j.scriptamat.2020.02.035>.
- (29) Liu, N.; Xie, Y.; Liu, G.; Sohn, S.; Raj, A.; Han, G.; Wu, B.; Cha, J. J.; Liu, Z.; Schroers, J. General Nanomolding of Ordered Phases. *Phys. Rev. Lett.* **2020**, *124* (3), 36102.  
<https://doi.org/10.1103/PhysRevLett.124.036102>.
- (30) Yu, H. B.; Luo, Y.; Samwer, K. Ultrastable Metallic Glass. *Adv. Mater.* **2013**, *25*, 5904–5908. <https://doi.org/10.1002/adma.201302700>.
- (31) Luo, P.; Cao, C. R.; Zhu, F.; Lv, Y. M.; Liu, Y. H.; Wen, P.; Bai, H. Y.; Vaughan, G.; Di Michiel, M.; Ruta, B.; Wang, W. H. Ultrastable Metallic Glasses Formed on Cold Substrates. *Nat. Commun.* **2018**. <https://doi.org/10.1038/s41467-018-03656-4>.
- (32) Annamareddy, A.; Voyles, P. M.; Perepezko, J.; Morgan, D. Mechanisms of Bulk and Surface Diffusion in Metallic Glasses Determined from Molecular Dynamics Simulations. *Acta Mater.* **2021**, *209*, 116794. <https://doi.org/10.1016/j.actamat.2021.116794>.
- (33) Zhang, P.; He, L.; Besser, M. F.; Liu, Z.; Schroers, J.; Kramer, M. J.; Voyles, P. M. Applications and Limitations of Electron Correlation Microscopy to Study Relaxation Dynamics in Supercooled Liquids. *Ultramicroscopy* **2017**, *178*, 125–130.  
<https://doi.org/10.1016/j.ultramic.2016.09.001>.
- (34) Pazmiño Betancourt, B. A.; Douglas, J. F.; Starr, F. W. String Model for the Dynamics of Glass-Forming Liquids. *J. Chem. Phys.* **2014**. <https://doi.org/10.1063/1.4878502>.

- (35) Chen, H.; Qu, B.; Li, D.; Zhou, R.; Zhang, B. Atomic Structure and Dynamics Properties of Cu<sub>50</sub>Zr<sub>50</sub> Films. *J. Appl. Phys.* **2018**, *123* (2). <https://doi.org/10.1063/1.5011122>.
- (36) Wu, C. Free Surface-Induced Glass-Transition Temperature Suppression of Simulated Polymer Chains. *J. Phys. Chem. C* **2019**. <https://doi.org/10.1021/acs.jpcc.9b01253>.
- (37) Yu, L. Surface Mobility of Molecular Glasses and Its Importance in Physical Stability. *Advanced Drug Delivery Reviews*. 2016. <https://doi.org/10.1016/j.addr.2016.01.005>.
- (38) Li, Y.; Zhang, W.; Bishop, C.; Huang, C.; Ediger, M. D.; Yu, L. Surface Diffusion in Glasses of Rod-like Molecules Posaconazole and Itraconazole: Effect of Interfacial Molecular Alignment and Bulk Penetration. *Soft Matter* **2020**. <https://doi.org/10.1039/d0sm00353k>.
- (39) Yu, H. Bin; Luo, Y.; Samwer, K. Ultrastable Metallic Glass. *Adv. Mater.* **2013**, *25* (41), 5904–5908. <https://doi.org/10.1002/adma.201302700>.
- (40) Segu, D. Z.; Choi, J. H.; Kim, S. S. Sliding Wear Behavior of Fe-Based Bulk Metallic Glass at High Temperature. *J. Mech. Sci. Technol.* **2012**, *26* (11), 3565–3570. <https://doi.org/10.1007/s12206-012-0855-z>.
- (41) Liu, L. F.; Zhang, H. A.; Shi, C. Sliding Tribological Characteristics of a Zr-Based Bulk Metallic Glass near the Glass Transition Temperature. *Tribol. Lett.* **2009**. <https://doi.org/10.1007/s11249-009-9410-1>.
- (42) Rahaman, M. L.; Zhang, L. C.; Ruan, H. H. Effects of Environmental Temperature and Sliding Speed on the Tribological Behaviour of a Ti-Based Metallic Glass. *Intermetallics* **2014**. <https://doi.org/10.1016/j.intermet.2014.03.011>.
- (43) Kumar, G.; Tang, H. X.; Schroers, J. Nanomoulding with Amorphous Metals. *Nature* **2009**, *457* (7231), 868–872. <https://doi.org/10.1038/nature07718>.

- (44) Thévenaz, P.; Ruttimann, U. E.; Unser, M. A Pyramid Approach to Subpixel Registration Based on Intensity. *IEEE Trans. Image Process.* **1998**. <https://doi.org/10.1109/83.650848>.
- (45) Sheng, H. W.; Ma, E.; Kramer, M. J. Relating Dynamic Properties to Atomic Structure in Metallic Glasses. *JOM* **2012**, *64* (7), 856–881. <https://doi.org/10.1007/s11837-012-0360-y>.
- (46) Plimpton, S. Fast Parallel Algorithms for Short-Range Molecular Dynamics. *J. Comput. Phys.* **1995**, *117* (1), 1–19. <https://doi.org/10.1006/jcph.1995.1039>.
- (47) Kob, W.; Andersen, H. C. Testing Mode-Coupling Theory for a Supercooled Binary Lennard-Jones Mixture. II. Intermediate Scattering Function and Dynamic Susceptibility. *Phys. Rev. E* **1995**, *52* (4), 4134–4153.

For Table of Contents Only

